RSC Advances

PAPER

View Article Online
View Journal | View Issue

Cite this: *RSC Adv.*, 2026, **16**, 3543

Flexible MXene nanosheet/multiwall carbon nanotube-reinforced poly (vinylidene fluoride-hexafluoropropylene)–polymethyl methacrylate composites for energy storage and EMI shielding

Nitesh Kumar Nath,[a] Rajanikanta Parida,[b] Bichitra Nanda Parida,[c] Dibyaranjan Das,[d] S. K. S. Parashar[d] and Nimai C. Nayak *[a]

Developing multifunctional materials that combine high energy storage capability with efficient electromagnetic interference (EMI) shielding remains a major challenge, as these properties often require conflicting structural features. In this work, we developed novel polymer-based nanocomposites (PNCs) using poly(vinylidene fluoride-*co*-hexafluoropropylene) (PVDF-HFP) and polymethyl methacrylate (PMMA) as the polymer matrix, reinforced with multi-walled carbon nanotubes (MWCNTs) and 2D $Ti_3C_2T_x$ MXene. This distinctive combination of MXene–MWCNT forms an interconnected 3D conductive network that not only enhances dielectric constant and electrical conductivity but also maximizes absorption dominated EMI shielding through multiple internal reflections. The formation of an interconnected conductive network facilitated efficient absorption and multiple reflections of incident electromagnetic waves. Interfacial polarization and Maxwell–Wagner–Sillars (MWS) effects elevate the dielectric constant for the 4 wt% nanocomposite film to 91.7 at 100 Hz. The 4 wt% nanocomposite film exhibited a total shielding effectiveness of 40.04 dB in the Ku band and 32.02 dB in the X band. Moreover, an enhanced energy density of 3.46 J cm^{-3} was achieved owing to improved charge–discharge efficiency. This work demonstrates a scalable route for designing lightweight, flexible PNCs with dual functionality, addressing the current gap between energy storage and EMI shielding applications.

Received 8th December 2025
Accepted 7th January 2026

DOI: 10.1039/d5ra09486k

rsc.li/rsc-advances

1. Introduction

The rapid advancement of portable electronics, wearable devices, flexible sensors, and next-generation communication systems has created a pressing demand for multifunctional materials that can simultaneously deliver high-performance energy storage and effective EMI shielding.[1] Traditional energy storage systems and shielding materials often fall short in terms of flexibility, weight, and adaptability to miniaturized architectures, which are now vital in modern technologies. Polymer-based nanocomposites (PNCs) with conductive nanofillers offer lightweight, flexible, and easily processed materials with customizable electrical and dielectric properties.[2] Among polymer candidates, PVDF-HFP and PMMA are particularly suitable for EMI shielding applications due to their exceptional dielectric constant, thermal stability, and processability.[3,4] PVDF-HFP, a semi-crystalline fluoropolymer, is well known for its high dielectric constant, electrochemical stability, and excellent mechanical flexibility. It also possesses strong dipole moments owing to the presence of $-CF_2$ groups, making it an attractive host for energy storage applications. PMMA, on the other hand, is an amorphous polymer known for its high transparency, rigidity, and excellent processability. Blending PVDF-HFP with PMMA yields a complementary balance of polarity, mechanical strength, and excellent film-forming properties.[5] However, the conductivity and EMI SE of these polymers are limited by their intrinsic insulating properties. An efficient method to improve the electrical conductivity and impedance matching of the composite is to incorporate highly conductive nanofillers, such as MWCNTs, graphene, carbon fibers (CFs) and MXene, into the polymer matrix.[6–8] MXenes, a novel class of 2D transition metal carbides, nitrides, and carbonitrides, have recently garnered exceptional attention for their remarkable electrical conductivity, high surface area, and rich surface functionalities.[9] MXene-only composites exhibit

[a]*Micro and Nano Materials Laboratory, Department of Chemistry, Faculty of Engineering & Technology (ITER), Siksha'O'Anusandhan (Deemed to be University), Khandagiri Square, Bhubaneswar, Odisha-751030, India. E-mail: nimainayak@soa.ac.in*

[b]*Department of Physics, Faculty of Engineering & Technology (ITER), Siksha'O'Anusandhan (Deemed to be University), Khandagiri Square, Bhubaneswar, Odisha-751030, India*

[c]*Central Institute of Technology, Kokrajhar (Deemed to be University, MHRD, Govt. of India) BTAD, Assam-783370, India*

[d]*Nanosensor Lab, School of Applied Sciences, Kalinga Institute of Industrial Technology (KIIT) Deemed to be University, Campus-3, Bhubaneswar, Odisha, 751024, India*

a high dielectric constant due to strong interfacial polarization, but MXene restacking at higher loadings increases dielectric loss and can cause impedance mismatch, limiting EMI shielding efficiency.[10] MWCNT-only composites show lower permittivity but achieve stable conductivity at low loadings, resulting in moderate, conduction-dominated EMI shielding with limited energy density.[11] It can effectively increase dispersion, prevent 2D layers from restacking, and help create a 3D interconnected filler network whenever combined with MXene.[12] In contrast, hybrid MXene–MWCNT composites combine high interfacial polarization with efficient conductive bridging, leading to enhanced dielectric constant and EMI shielding effectiveness while maintaining controlled dielectric loss. The 50 : 50 ratio of MXene to MWCNT was initially chosen based on preliminary trials and literature reports indicating that equal proportions often provide a balanced synergy between conductivity (from MWCNT) and surface area/interface effects (from MXene).[13,14] The performance of dielectrics and EMI shielding depends on interfacial polarization, which is improved by such synergy in addition to improving charge transport.[15] The utilization of two or more conducting filler particles with large specific surface areas and high aspect ratios can benefit from their synergistic impact, which can also lower the percolation threshold and improve the EMI SE of the PNCs. Numerous investigations have studied absorption-dominated effective shielding characteristics MXene based PNCs.[16]

The 2D $Ti_3C_2T_x$ filled PVDF composite was investigated by K Rajavel *et al.*.[17] The resultant nanocomposite showed a remarkable EMI SE of 48.47 ± 3.5 dB for 22.55 vol% filler concentrations at a thickness of 2 mm. PVDF/MWCNTs composites were successfully created by Wang *et al.* using hot compression molding and mechanical mixing. In the X-band frequency spectrum, the samples with a 7 wt% percent filler content had conductivity and SE of 6 S m^{-1} and 30.89 dB, respectively.[18] The EMI shielding composites of CNT/graphene nanoplatelet (GNP)/poly (ε-caprolactone) (PCL), CNT/CB/PCL, and CB/GNP/PCL were prepared by Sun *et al.*[19] The combined effects of CNT, GNP, and CB produced microwave shielding effectiveness values of 53.8 and 54.6 dB, respectively. An ultrathin and flexible carbon nanotube/MXene/cellulose nanofiber composite paper, a gradient and sandwich-structured paper, was developed by Cao *et al.* using basic alternating vacuum-assisted filtration technology.[20] It demonstrated a high conductivity of 2506.6 S m^{-1} and a high EMI SE of 38.4 dB. Zhao *et al.*[21] synthesized PVDF/GNP foams using the basic intermittent foaming approach and examined their conductivity and EMI shielding performance. The maximum conductivity of 0.52 S m^{-1} and EMI SE of roughly 27 dB were demonstrated by 10 wt% GNP foam, which had a porosity of 48.7%. Zhang *et al.*[22] reported that a multifunctional PMMA/Fe_3O_4@MWCNTs composite foam with an EMI SE of 13.1 dB was created using the supercritical carbon dioxide ($ScCO_2$) foaming process. Liang *et al.* used solution casting and hot pressing to create a graphene/Ni chain/PVDF multilayer composite.[23] The homogeneous composite exhibits the greatest EMI SE of 43.3 dB at 0.5 mm thickness in terms of both reflection and absorption. According to Al-Ghamdi *et al.*,[24] poly (vinyl chloride)/graphite nanosheet/nickel (PVC/GN) nanocomposites exhibited a maximum EMI SE of 47 dB in the microwave frequency range. Similarly, Priyanka *et al.*[25] reported that PVDF/carbon black (CB) nanocomposites with 10 wt% CB loading achieved maximum EMI SE values of approximately −11.1 dB in the X-band and −11.5 dB in the Ku-band. It is well known that improving the conductive filler content or thickness will enhance its EMI SE performance at the expense of its ductility and flexibility.[26] Therefore, several structural designs were investigated in order to enhance the EMI SE performance of flexible composites while maintaining their electrical properties.[27] It is noteworthy that the structural design strategies employed to enhance the breakdown strength and energy storage density of PVDF-based nanocomposites such as the incorporation of high permittivity ceramics and high aspect ratio conductive fillers also play a pivotal role in improving EMI shielding performance. According to Luo *et al.*, P(VDF-HFP)/PMMA blend films containing 42.6 vol% PMMA achieved a discharged energy density of 11.2 J cm^{-3} with an efficiency of 85.8% at an electric field of 475 MV m^{-1}.[28] Cheng *et al.* fabricated GO/P(VDF-CTFE) composite films *via* a casting process by incorporating graphene oxide (GO) into poly (vinylidene fluoride-*co*-chlorotrifluoroethylene) [P(VDF-CTFE)]. At an applied electric field of 3400 kV cm^{-1}, the composite containing 0.4 wt% GO nanosheets exhibited a discharged energy density of 8.25 J cm^{-3} and a dielectric constant of 13.6 at 1 kHz.[29] At room temperature and an applied electric field of 400 MV m^{-1}, the maximum electric displacement reaches 10.96 μC cm^{-2}, while the discharged energy density achieves 17.22 J cm^{-3} reported by Wang *et al.*.[30] The remarkable energy density (U_e) of 16.9 J cm^{-3} at 370 kV mm^{-1} is achieved by the trilayered PVDF/Ta–Al@TiO_2 nanoparticle/BT single-crystal platelet nanocomposite film, which is an improvement of almost 625% over the single-layer film reported by Li *et al.*.[31] Wang *et al.* shows that, the incorporation of MWCNTs into the CCTO/PVDF composite increased the energy storage density from 0.617–1.395 J cm^{-3}, representing more than a twofold enhancement.[32] The majority of earlier research typically optimizes either EMI shielding or energy storage performance, our work achieves simultaneous enhancement of both, providing a multifunctional platform for electronic devices.[33,34] Although the application of flexible nanocomposites in energy storage and EMI shielding is still in its infancy, our study uniquely integrates these two functionalities within a single material system.

In this work, flexible MXene–MWCNT reinforced PVDF-HFP/PMMA nanocomposite films are fabricated *via* solution blending to simultaneously enhance energy storage density and EMI shielding in a single film. The hybrid architecture improves filler dispersion, interfacial interactions, and conductive network formation, enabling efficient shielding across a broad frequency range and multifunctional performance for next-generation electronics.

2. Experimental section

2.1. Materials

PMMA (marketed under the trade name VH 001) and PVDF (marketed under the brand name Kynar 720) were provided by HI

Media Laboratories Pvt. Ltd. We purchased MWCNT powders from Iljin Nanotech Co., Ltd. (South Korea) with dimensions of 10–20 nm, lengths of 0.5–15 μm, and purity levels more than 95%. *N*,*N*-Dimethylformamide (DMF) was provided by Macron Fine Chemicals and used to make composites samples. We bought the 98.0% AR quality Ti_3AlC_2 MAX phase powder from Forsman Scientific Co., Ltd. in Beijing, China. A 40.0% concentrated hydrofluoric acid (HF) solution of AR grade was provided by Qixian Huihongyuan Chemical Co. Ltd. (Shanxi, China). Sigma Aldrich in India supplied the sulfuric acid (H_2SO_4, > 97%, AR grade) and nitric acid (HNO_3, 37%, AR grade).

2.2. Functionalization of $Ti_3C_2T_x$ & f-MWCNTs

Ti_3AlC_2 powder is used to extract Al selectively by adding it to a 40% HF solution and stirring it for 24 hours at room temperature. The etched solution is centrifuged after being repeatedly washed with DI water until the pH reaches about 5–6. A few-layered MXene is produced by sonicating the etched $Ti_3C_2T_x$ in DMSO to further separate the layers. $Ti_3C_2T_x$ MXene powder is obtained by filtering and vacuum-drying the final suspension. The pristine MWCNTs (*p*-MWCNTs) are refluxed for 12 hours at 60 °C in a 3 : 1 H_2SO_4 : HNO_3 mixture, adding –COOH and –OH groups. The resulting acid-treated dispersion was subsequently diluted with ethanol and deionized water, followed by repeated washing and filtration until a neutral pH was achieved.

2.3. Preparation of nanocomposite film

A PVDF-HFP/PMMA blend (50 : 50 wt%) is prepared by dissolving both polymers in DMF at 60 °C under constant stirring for 2 h. MXene–MWCNT nanofillers (1 : 1 wt. ratio and 0.5, 1, 2, and 4 wt% relative to the total polymer weight) are dispersed in DMF by ultrasonication for 30 min and subsequently incorporated into the polymer solution, followed by stirring for 8 h. The ratio between MXene and MWCNTs was selected based on preliminary trials and supported by literature-reported synergistic effects. Multiple compositions were initially screened to assess processability, dispersion stability, and network formation. The chosen proportion provided an optimal balance and uniform dispersion, while minimizing aggregation and phase separation. In order to reduce MXene oxidation during film casting, the MXene was handled at room temperature and blended with the polymer solution right away to minimize exposure to moisture and air. Furthermore, the encapsulation in the PVDF-HFP/PMMA matrix acts as a barrier to prevent direct contact with water and oxygen, which slows oxidation. The mixture is then cast onto a Teflon plate and dried at 80 °C. The resulting films, with a thickness of 0.35 mm, are used for subsequent characterization. Fig. 1 presents a schematic illustration of the synthesis of the nanocomposite. This Fig. S1 depicts the formation mechanism, interfacial interactions, and conductive network architecture in the polymer nanocomposite.

2.4. Characterization of sample

Initial investigation was conducted using an XRD equipment (Model: Rigaku Ultima IV, Japan), FT-IR (Jasco FT-IR-4600 TYPE-A). The microstructure was examined at room temperature using

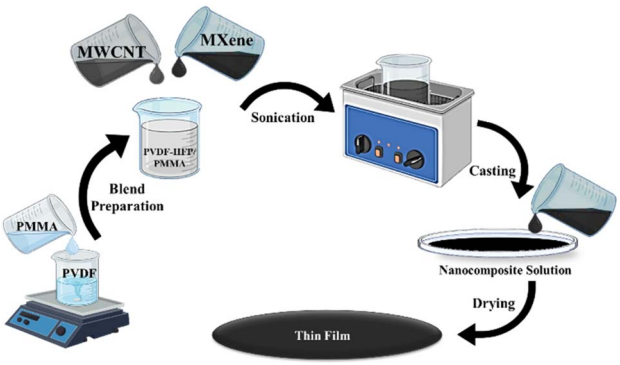

Fig. 1 Schematic illustration of the synthesis process of the nanocomposite.

an Oxford Instruments MFP-3D Origin microscope and an EVO-18 Carl Zeiss Field Emission Scanning Electron Microscope. The dielectric properties were measured using an LCR meter (Model: PSM-1735, LCR N4L, UK) in the temperature range of 25–100 °C. The electrical impedance properties of the resulting composites were evaluated using a Hioki-Impedance Analyzer IM3570 electrical impedance analyzer (100 Hz to 5 MHz). A Marine India *P*–*E* loop tracer was used to test the ferroelectric behavior at ambient temperature. The Rohde & Schwarz ZNB-20 VNA (Vector Network Analyzer) is used to assess the electromagnetic interference (EMISE) and material properties of composite film, particularly their electrical and magnetic characteristics, within the Ku-band (12–18 GHz).

3. Results and discussion

3.1. Crystallinity and phase identification

The characteristics of functionalized 2D $Ti_3C_2T_x$ MXene and 1D MWCNTs are provided in the SI file (Fig. S2). Fig. 2(a) displays the XRD pattern of the sample made using the solution casting method. The dominant PVDF β-phase reflection at $2\theta \approx 20.3°$ corresponds to the (110) planes. The addition of PMMA generally reduces crystallinity due to its amorphous nature, leading to broadening of these peaks. A hybrid structure with both crystalline and amorphous parts is suggested by the combination of broad and sharp peaks. The existence of multilayer MXene within the polymer matrix is indicated by the distinctive (002) peak of $Ti_3C_2T_x$ which arises at about 6.45°. A shift or broadening of this peak signifies effective interaction and dispersion within the polymer.[35] A noticeable diffraction peak in MWCNTs is situated at roughly 26.0°, which is equivalent to the graphitic (002) plane. If MWCNTs are evenly distributed throughout the polymer matrix, this intensity of peak may decrease. The addition of MXene and MWCNTs usually reduces peak intensity by limiting molecular chain mobility, which changes the overall crystallinity PNC films. A loss of crystallinity and peak broadening are indicated by the significant interaction between the polymer chains and nanofillers. The appearance of the additional (100) and (021) MXene reflections in the red spectrum is primarily associated with the structural ordering of $Ti_3C_2T_x$ MXene sheets. However, this ordering is indirectly influenced

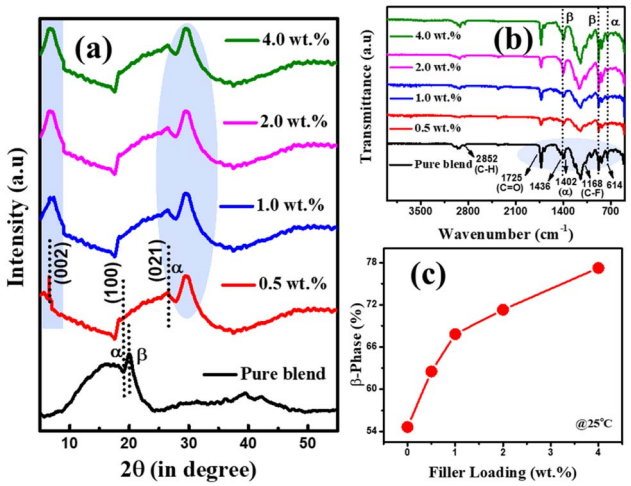

Fig. 2 (a) XRD spectra of PNC films varying filler concentration (b) FT-IR spectra (c) β-phase percentage varying filler concentration of PNC films.

by the existence of MWCNTs. During solvent evaporation, the 1D MWCNTs can cause partial alignment and controlled restacking of MXene sheets by acting as spacers and conductive bridges between neighboring MXene layers.[36] These interactions have an impact on the dielectric and ferroelectric characteristics. The IR spectroscopy of PNC films validate robust interactions between the nanofillers and the polymer matrix, resulting in notable structural and phase changes. The distinctive peaks of PVDF-HFP can be seen in the FTIR spectra at around 840 cm^{-1} (β-phase) and CF_2 stretching at 1168 cm^{-1}, as well as C=O stretching from PMMA at about 1725 cm^{-1} (Fig. 2(b)). The successful inclusion of the nanofillers is further confirmed by peaks related to MWCNTs (~1570 cm^{-1} for C=C stretching) and $Ti_3C_2T_x$ MXene (~600–800 cm^{-1} for Ti–C vibrations). Strong interfacial interaction and hydrogen bonding between the matrix and the nanofillers are suggested by slightly shifts in the CF_2 and C=O peaks. Several investigations have shown that MXene interact with the molecular dipoles (CF_2) of PVDF-HFP to increase the β-phase concentration of composites.[37]

The Gregorio & Cestari equation below can be used to get the β-phase (F_β) percentage:[38]

$$F(\beta) = \frac{A_\beta}{1.26 \times (A_\alpha + A_\beta)} \quad (1)$$

where A_α and A_β stand for the respective absorption coefficients for the β-phase (840 cm^{-1}) and the α phase (762 cm^{-1}). The concentration of nanofillers in the matrix are displayed with the percentage of the β phase in the plot in Fig. 2(c). The maximum β phase that was attained was nearly 77% for 4 wt% composite film. All of these interactions work together to improve the dielectric characteristics, increase the β-phase content, and boost the functional performance. The hydrogen atoms of $-CH_2$ in PVDF-HFP and the oxygen atom of the carbonyl group in PMMA may form a weak C–H–O hydrogen bond, despite the fact that neither PVDF-HFP nor PMMA have traditional hydrogen bond donors like –OH. It is possible for these modest interactions to suppress phase separation and encourage interfacial adhesion. The Raman spectra (Fig. S3) show characteristic MXene vibrational modes in the 4 wt% filler-loaded composite, confirming the presence and structural integrity of MXene and MWCNTs within the polymer matrix.

3.2. Microstructural analysis

The surface morphology, nanofiller dispersion, and structural integrity are all thoroughly examined by FESEM analysis. A well-distributed and interconnected network of MWCNTs and $Ti_3C_2T_x$ within the polymer matrix is seen which, ensuring improved stability and electrical conductivity. The PVDF-HFP/PMMA blend has a smooth phase-separated structure as seen in Fig. 3(a). A layered morphology is created by adding MXene, which has a 2D sheet-like structure. MWCNTs are uniformly distributed throughout the polymer as entangled tubular structures that create conductive pathways, as depicted in Fig. 3(b and c). In order to prevent polymer over-coating of individual fillers and maintain a continuous co-network within the PVDF-HFP/PMMA matrix, we pre-assemble MXene–MWCNT and use a segregated-network casting route. This allows us to maintain high conductivity and absorption-dominated EMI shielding without compromising dielectric performance.

The surface of the composite film exhibits limited filler aggregation, suggesting robust interfacial interactions that enhance flexibility and electrical performance. Interfacial adhesion is strengthened by the presence of MXene layers, while enhanced charge storage and EMI shielding capabilities are suggested by the porosity microstructure seen in some areas. Fig. 3(d and e) presents the elemental color mapping images and corresponding EDX spectra of the composite films, confirming the uniform distribution of fillers within the polymer matrix.

3.3. Dielectric analysis

The influence of varying nanofiller weight fractions within the matrix on the electrical properties was systematically examined to develop composite materials with enhanced dielectric

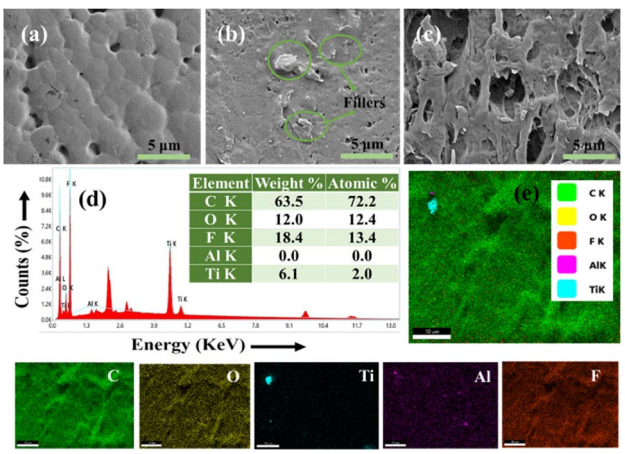

Fig. 3 (a) FE-SEM image of pure blend (b and c) Surface and cross-sectional image of PNC films, respectively (d) EDAX of composite film (e) color mapping of NCs.

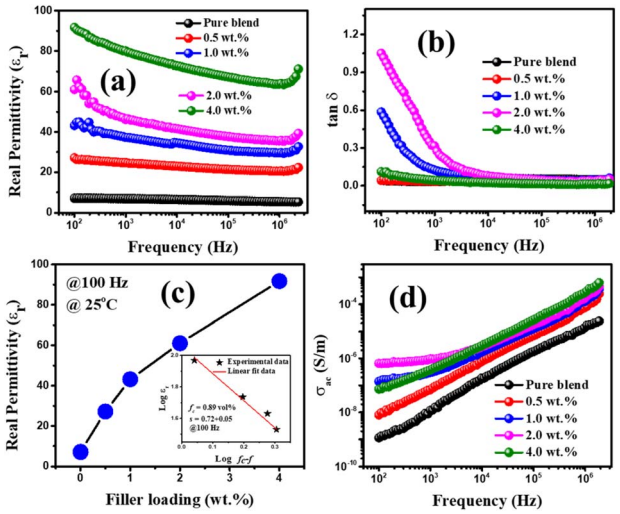

Fig. 4 (a) Frequency dependent ε_r (b) tan δ (c) ε_r *vs.* Filler loading at 100 Hz (inserted figure is a fitted plot of the percolation threshold) (d) σ_{ac} at different frequency for PNC films.

performance. The frequency-dependent dielectric permittivity of the PNC films at 25 °C in the 100 Hz to 1 MHz frequency range is shown in Fig. 4. The dielectric constant (ε_r) of a substance is directly proportional to the capacitance, which is expressed mathematically by:

$$\varepsilon_r = \frac{l \times C_p}{A \times \varepsilon_0} \quad (2)$$

where A represents the area of PNCs, l is thickness, ε_0 is permittivity in free space (8.854×10^{-12} F m^{-1}), and C_p its parallel capacitance. The 4 wt% composite film has a high permittivity value of 91.7 at 100 Hz which is nearly 12 times greater than the pure PVDF-HFP/PMMA blend, as seen in Fig. 4(a). MWS polarization is responsible for the significant rise in dielectric permittivity at low frequencies, which is accompanied by an increase in dielectric loss. The permittivity gradually decreases with increasing frequency, reflecting the declining contribution of interfacial charge accumulation. At higher frequencies, where interfacial charges cannot follow the alternating field, the dielectric response is dominated by dipolar and intrinsic polarization mechanisms.[39] The dielectric loss is typically considerable at low frequencies, particularly at interfaces between the polymers and fillers. This is a common phenomenon in composites where localized charge accumulation is caused by heterogeneity. The composite with a 4 wt% filler component has a decent loss value of 0.11 at 100 Hz, according to Fig. 4(b). The loss (tan δ) decreases with increasing frequency because dipolar polarization is unable to keep up with the rapidly changing field. The dielectric behavior of the composites was predicted using the traditional percolation theory.[40,41] The following power laws can be used to determine the ε_r of PNCs that are near the percolation threshold:

$$\varepsilon_r = (f_c - f)^{-s} \text{ for } f < f_c \quad (3)$$

where s is the critical or power law exponent related to the properties of the material, f is the volume fraction of nanofiller, and f_c is the percolation threshold. The calculation shows that s is 0.72 and fc is 0.89 vol% (almost 3.15 wt%). This was ascertained by linearly fitting Log ε_r *vs.* Log$(f_c - f)$, as shown in Fig. 4(c). The dielectric constant remains very close to the polymer matrix at low filler concentrations but significantly increases at larger concentrations, especially in closer proximity of the percolation threshold. A conductive network starts developing at this threshold, which causes permittivity to rise significantly. The electrical conductivity (σ_{ac}) of PNCs with varying filler concentrations is plotted against frequency in Fig. 4(d). The following is the mathematical expression for σ_{ac}:

$$\sigma_{ac} = \omega \varepsilon_0 \varepsilon_r \tan \delta \quad (4)$$

The conductivity of the composites with a filler loading of 0.5 wt% remained low because the absorbed insulating polymer chains function as the dielectric barrier regulating tunneling conduction and prevent full contact between the clusters of nanoparticles. In accordance with the minimal dielectric loss, the conductivity increased from 1.14×10^{-9}–6.57×10^{-7} S cm^{-1} at 100 Hz, suggesting that no conducting route was established in the composites. Due to the insulating nature of the matrix, interfacial polarization predominates and charge mobility is restricted at low frequencies, as seen by the relatively constant or slightly increased AC conductivity.[42,43] On the other hand, charge carrier hopping or tunneling between conductive filler sites is responsible for the notable increase in conductivity at higher frequencies.

Fig. S4(a and b) shows the strong temperature dependence of ε_r and σ_{ac} in the PVDF-HFP/PMMA composite containing 4 wt% nanofillers, which can be attributed to thermally activated charge transport mechanisms.[44] The enhanced mobility of polymer chains and dipolar segments is responsible for the gradual rise in the dielectric constant with temperature, which improves orientation polarization. Similarly, the σ_{ac} rises with temperature in an Arrhenius-type manner since thermal energy makes it easier for charge carriers to tunnel between conductive filler sites. The composite exhibits a good combination of rising conductivity and dielectric constant with temperature, suggesting that it could have high-performance uses in energy storage and temperature-sensitive electronic devices.

3.4. Impedance analysis

Impedance analysis of composites at different filler loading provides crucial information about the interfacial behavior and electrical transport of the material. The complex impedance (Z^*) is analyzed using the following equation:

$$Z^* = Z - jZ'' = \frac{R}{1 + (\omega RC)^2} - j\frac{\omega R^2 C}{1 + (\omega RC)^2} \quad (5)$$

where Z' and Z'' represent the real and imaginary components of Z^*, ω is angular frequency, C is capacitance, and R is resistance. The impedance (Z) represents the overall frequency-dependent response of the material, reflecting the combined resistive and capacitive contributions. The semicircular arc at

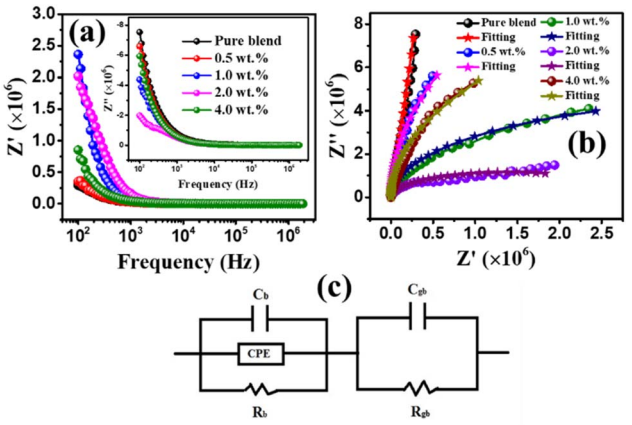

Fig. 5 (a) Frequency dependent Real and Imaginary impedance spectra (inserted) (b) The Nyquist plot for PNC films with circuit fitting (c) CQR-CR fitting parameter.

high frequencies is followed by a tail or inclined line at lower frequencies in the complex impedance spectra, which are depicted in Fig. 5(a). The low-frequency portion denotes interfacial polarization and electrode effects, whereas the high-frequency semicircle represents the bulk resistance and capacitance of the PNC films. A single depressed semicircle indicates that the heterogeneous structure leads to a non-ideal Debye-type relaxation.[45,46] The semiconductor hypothesis is supported by the depressed arcs seen in the Nyquist plot (single relaxation process). A combination of resistive and non-ideal capacitive responses is suggested by the impedance behavior, which is frequently represented by comparable circuits with resistors and constant phase elements.

Fig. 5(b) displays the Nyquist plots jointly with the corresponding CQR-CR fitting parameter (as shown in Fig. 5(c)). The impedance spectra were fitted using a CQR-CR equivalent circuit, where C_1 and R_1 represent the bulk dielectric response of the polymer matrix, Q (CPE) accounts for non-ideal capacitive behavior arising from interfacial polarization and filler dispersion, and C_2–R_2 correspond to electrode–polymer interfacial effects. The CPE exponent ($n < 1$) confirms deviation from ideal Debye behavior. The development of partial conductive channels, which facilitate charge transport while preserving capacitive properties, is facilitated by the presence of MXene and MWCNTs. The complete equivalent circuit model used for impedance fitting along with the corresponding fitting parameters are presented in Table S1.

4. Application

4.1. EMI shielding effectiveness analysis

The EMI shielding materials act as a protective covering for electronic devices, preventing undesired electromagnetic radiation (EMR) leakage from the gadgets. Since EMI might interfere with these applications, it is crucial to create high-performance, lightweight shielding materials. The PNC film is an excellent choice due to its strong electrical conductivity, low dielectric loss, and good ferroelectric properties, all of which help to effectively shield against electromagnetic interference.[47] The S-parameters of the composite films like input reflection coefficient data (S_{11}), forward transmission coefficient data (S_{21}), reverse transmission coefficient data (S_{12}), and output reflection coefficient data (S_{22}) were measured using a VNA. The values of T, R, and M can affect the value of EMI SE_T in the following ways:[48]

$$R = |S_{11}|^2 = |S_{22}|^2 \quad (6)$$

$$T = |S_{21}|^2 = |S_{12}|^2 \quad (7)$$

The sum of R, T, and A equals 1. The sum of the effectiveness resulting from absorption (SE_A), reflection (SE_R), and multiple internal reflection (SE_M) is known as the total shielding effectiveness (SE_T).

$$SE_T = SE_A + SE_R + SE_M \quad (8)$$

The contribution of SE_M can be neglected if SE_A reaches 10 dB due to the energy from these reflections is absorbed as heat. Consequently, the overall SE of a material can be written as:

$$SE_T = SE_A + SE_R \quad (9)$$

The following expression is used to calculate the values of (SE_A) and (SE_R):

$$SE_R = -10\log(1 - R) \quad (10)$$

$$SE_A = -10\ \log\left[\frac{T}{1 - R}\right] \quad (11)$$

where R is the reflection coefficient and T is the projection coefficient. If SE_A is greater than 10 dB then SE_M can be ignored. Fig. 6(a, e), (b, f), and (c, g) present the values of SE_A, SE_R and SE_T for the composites in the X band and Ku bands, respectively. In the X-band, the maximum SE_A is roughly 19.11 dB at 8 GHz, the maximum SE_R is 12.86 dB at GHz, and the SE_T is reaches about 32.02 dB at 8 GHz for 4 wt% composite film. The maximum SE_A in the Ku-band is around 23.05 dB at 17.5 GHz, the maximum SE_R is around 16.9 dB at 17.5 GHz, and the SE_T reaches around 40.04 dB at 17.5 GHz. The standard deviation associated with SE_T is 8.02. The primary explanation is the noticeably smaller reflection component SE_R in the Ku band, which is compensated by a marginal increase in absorption, thereby raising the overall SE_T. Reflection is the mechanism by which part of an EMR is reflected when it first interacts with the PNCs in order to interact with the mobile charge carriers. Once the residual wave has entered the composite and interacted with free electrons, resulting in magnetic and dielectric loss and a loss of electromagnetic energy.[49] Additionally, the intensity of EMR is significantly decreased when facing the film, and this procedure is repeated for each individual that makes up the system. This might result in multiple internal reflections and ultimately dissipate as heat due to numerous dielectric losses in multilayer structures. The majority of the re-reflected waves are absorbed if the SE_A is more than 10 dB.[50] The experimentally determined EMI SE_T of the multilayer films increases

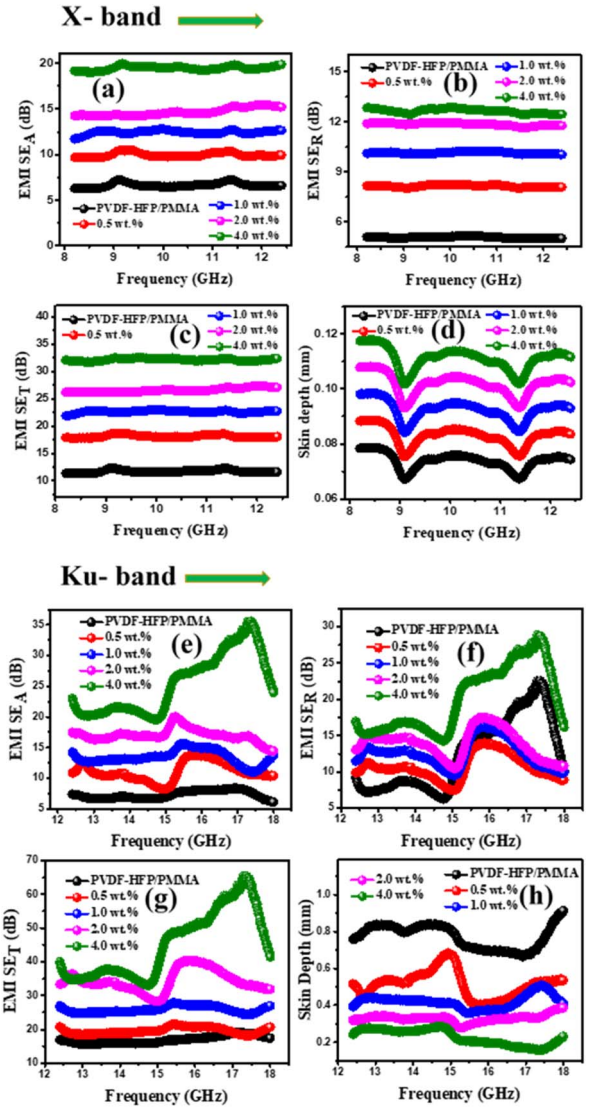

Fig. 6 Frequency dependent (a) SE_A (b) SE_R (c) total EMI shielding effectiveness (SE_T) (d) skin depth (δ) value in the X band and (e) SE_A (f) SE_R (g) total EMI shielding effectiveness (SE_T) (h) δ value in the Ku band of the nanocomposite films.

progressively from 16.92–40.04 dB in the Ku band and from 11.38–32.02 dB in the X band as the filler concentration rises from 0 to 4 wt%. An increase in the SE_T is directly correlated with an increase in the electrical conductivity of composite materials. Many electrons or holes were present, acting as extremely mobile charge carriers that interacted with the external electromagnetic field with remarkable mobility. As the filler content increased, the interconnected conductive network reached percolation, significantly increasing conductivity and improving attenuation of incident electromagnetic waves. MWCNTs Offer a network of conductive percolation, increasing the effectiveness of shielding.

The conductivity plots for the 4 wt% composite film in the X band (8–12 GHz) and Ku band (12–18 GHz) are provided in the supplementary information as Fig. S5(a and b). Despite its low DC conductivity, the 4 wt% nanocomposite film attains high shielding effectiveness because, at GHz frequencies, conductivity is significantly enhanced by interfacial polarization, hopping relaxation, and multiple internal reflections, resulting in absorption dominated attenuation.[51,52] The frequency dependent loss tangent was used to study dielectric behavior in the GHz regime as shown in Fig. S3(c and d). The low loss characteristic at GHz frequencies minimizes dielectric heating and maintains stable capacitive performance under high-frequency operation. The combination of moderate dielectric loss and enhanced conductivity promotes absorption, enabling superior shielding effectiveness (>40 dB in Ku-band) without compromising stability. The absorption component of EMI shielding is primarily enhanced by increasing thickness at constant filler loading up to a few skin depths, after which it becomes saturated. Therefore, the key to optimizing absorption-dominated SE_T with minimal added mass is to balance thickness with impedance matching and interfacial loss. In the current study, the composite exhibits a SE_R value of approximately 8.17 dB in the X band and 10 dB in the Ku band at a 0.5 wt% nanofiller concentration. The increase in SE_R can be attributed to the frequency dependent nature of different polarization mechanisms atomic, electronic, and dipolar polarization. At higher frequencies, these polarizations contribute to enhanced impedance mismatch at the air material interface, leading to greater reflection of incident electromagnetic waves.[53,54] The probable mechanism of transmission and absorption by several reflections are depicted in Fig. 7. However, it is significant that this increment in absorption value is actually more than that of MWCNT-based nanocomposites. The addition of more amount of nanofillers greatly enhanced both SE_T and SE_A in the case of all PNCs, whereas contribution of SE_R is minimal. In both the X- and Ku-bands, the composite demonstrates remarkable EMI shielding performance, attributed to enhanced reflection, facilitated wave penetration for

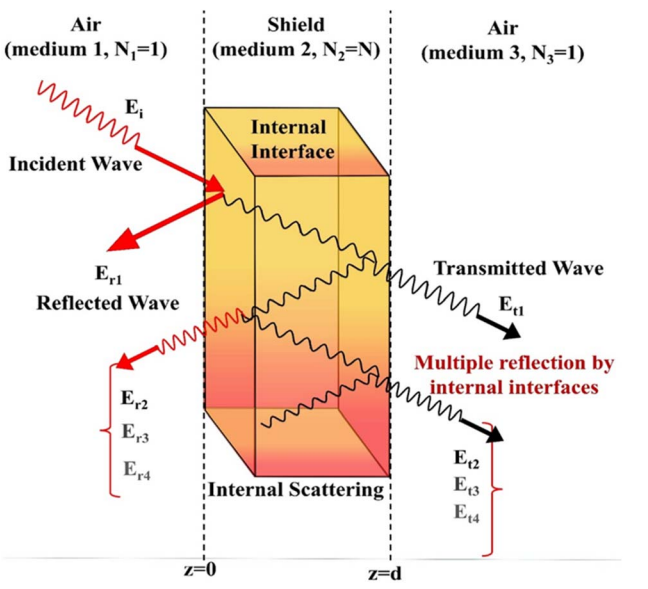

Fig. 7 An illustration of the electromagnetic shielding mechanism for composite film.

absorption, and efficient electromagnetic wave dissipation. Table S2 presents a comparison of the EMI shielding effectiveness (SE_T) of various polymer composites incorporating conductive filler.

Since electrical conductivity and EMI SE are known to be positively interconnected to each other. The distance within a conductor at which the intensity of electromagnetic waves decreases to 1equivalent to its initial value at the surface is known as the skin depth (δ). It establishes the depth to which an electromagnetic wave can penetrate into a material.[55] It is mathematically defined as:

$$\delta = \sqrt{\frac{1}{\pi f \mu \sigma}} = \frac{8.68 \times \text{thickness of material}}{SE_A} \quad (12)$$

where, f, μ ($4\pi \times 10^{-7}$ H m^{-1}) and σ are frequency, permeability and electrical conductivity, respectively. As shown in Fig. 6(d and h), the minimum skin depth (δ) was found to be 0.09 mm in the X band and 0.24 mm in the Ku band, indicating that absorption is the dominant shielding mechanism in both frequency ranges. Although the measured DC conductivity of the 4 wt% composite is relatively low, the effective AC conductivity at GHz frequencies is significantly higher, arising from different types of polarization and multiple internal reflections. This increase in σ_{ac} leads to a significant reduction in skin depth, particularly in the Ku band, which corresponds with the observed rise in SE_T when moving from the X band to the Ku band. Thus, the smaller effective penetration depth at higher frequencies, combined with strong interfacial polarization effects, underpins the superior absorption-dominated EMI shielding performance of the composites. These results confirm that the flexible PVDF-HFP/PMMA based composite film is a promising material for lightweight, high-performance EMI shielding applications in advanced electronics and wearable devices.

4.2. Polarization-electric field analysis

The ferroelectric behavior has been studied to evaluate its potential for multipurpose uses, such as flexible electronics, sensors, and adjustable EMI shielding systems. The polar β-phase rich PVDF-HFP matrix provides strong dipolar polarization under an alternating electromagnetic field. At microwave frequencies, these dipoles contribute to dipolar relaxation losses, which act synergistically with conduction loss from MXene/MWCNT networks. This cooperative loss mechanism enhances electromagnetic wave attenuation within the bulk of the composite, thereby favoring absorption-dominated shielding rather than reflection.[56] In order to restore and improve the ferroelectric response, these nanofillers are essential due to its extensive surface functionalities (–OH, –F, =O). MXene promotes nucleation of the β-phase by facilitating strong interfacial contacts with the polymer chains. In order to help dipole alignment during electrical poling, MWCNTs build conductive networks and produce localized electric fields.[57] On the other hand, more dielectric loss may result from excessive conductive filler loading. PMMA has a crucial regulatory role in this situation. It functions as a dielectric-moderating and dispersion-assisting phase since it is a low-loss, non-ferroelectric polymer. The composite consequently displays an enhanced Polarization–Electric field (P–E) hysteresis loop, which is distinguished by a decrease in the coercive field (E_c), a rise in the saturation polarization (P_s), and an increase in the remnant polarization (P_r), as illustrated in Fig. 8(a). The area enclosed between the charging and discharging curves (Fig. S6) of the P–E loop is also used to determine discharged energy density (U_d) according to the following equation:[58]

$$U_d = \int_{P_r}^{P_{max}} E dp \quad (13)$$

$$U_{total} = \int_{0}^{P_{max}} E dp \quad (14)$$

$$\eta = \frac{U_d}{U_{total}} = \frac{W_1}{W_1 + W_2} \times 100 \quad (15)$$

where U_{total} stand for total energy storage, η is the energy storage efficiency, W_1 and W_2 represent the discharged and lost energy density, respectively. As seen in Fig. 8(b), the corresponding discharged energy density and storage efficiency for 4 weight percent composite film at 5 KV cm^{-1} are 3.46 J cm^{-3} and 78.6%, respectively, suggesting minimal energy loss during the cycle. The composite offers not just a high energy density but also a high-power density, which indicates that the quick discharge. The high energy density and observed dielectric constant suggest that it may store a significant amount of electrical energy with minimal loss, making it suitable for high-energy density capacitors. The synergistic interaction between MXene and MWCNTs in polymer matrix forms a robust and highly functional dielectric network, making it well-suited for advanced capacitor applications. The integrated enhancements in energy density, and polarization behavior of composite demonstrate the potential for high-performance EMI shielding systems, flexible electronics, and energy storage, among other multipurpose applications.

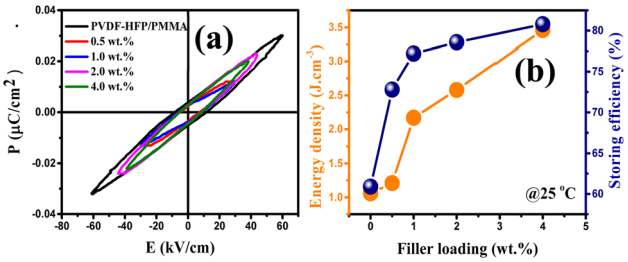

Fig. 8 (a) Ferroelectric hysteresis loop of PNC films (b) discharged energy density and energy storing efficiency of composite film, respectively.

5. Summery and conclusion

The study shows MXene–MWCNTs reinforced PVDF-HFP/PMMA nanocomposites were successfully fabricated, demonstrating simultaneous enhancement of ferroelectric, dielectric, and EMI shielding performance. The synergistic interaction

between 2D MXene nanosheets and 1D MWCNTs within the polymer blend promoted improved interfacial polarization, space charge accumulation, and dipolar orientation, resulting in a significantly higher dielectric constant (91.7 at 100 Hz) with reduced dielectric loss at optimal filler loadings. Impedance and conductivity analyses confirm that effective conductive pathways develop without compromising the insulating qualities of the pure matrix, especially around the percolation threshold. Additionally, temperature-dependent studies reveal thermally activated charge transport and stable dielectric behavior, further supporting their performance in dynamic environments. The prepared material exhibits strong absorption properties for EMI shielding, with an absorption efficiency (SE_A) of approximately 19.15 dB in the X band and 23.02 dB in the Ku band, and a total shielding effectiveness (SE_T) of about 32.02 dB at 8.5 GHz (X band) and 40.04 dB at 12.5 GHz (Ku band). These results highlight a viable pathway for designing multifunctional polymer nanocomposites with balanced high permittivity, low dielectric loss, and tunable conductivity, making them promising candidates for microwave absorption and EMI shielding applications.

Author contributions

The manuscript was written through contributions of all authors. All authors have given approval to the final version of the manuscript.

Conflicts of interest

The authors declare that they do not have no relevant financial or nonfinancial interest to disclose.

Data availability

Data will be available on request.

Supplementary information (SI): additional experimental details, such as characterization data (XRD, FT-IR, Raman, FESEM), conductivity analysis, ferroelectric (*P–E* loop) measurements, EMI shielding performance data, supplementary figures and tables. See DOI: https://doi.org/10.1039/d5ra09486k.

Acknowledgements

The authors declare that no funds, grants, or other support were received.

References

1 R. Cui, Y. Li, X. Zhang, Z. Duan, B. Zhao and C. Wan, Controlled deintercalation of graphene/organic superlattices with dense atomic-scale steric Schottky heterojunctions for extreme microwave absorption, *Nat. Commun.*, 2025, **16**(1), 5804.

2 M. GM, P. Dixit, R. H. Krishna and G. K. S, Polymer based composites for electromagnetic interference (EMI) shielding: The role of magnetic fillers in effective attenuation of microwaves, a review, *Hybrid Adv.*, 2024, **6**, 100200.

3 M. Iftikhar, F. Shahzad, J. Ahmad and X. Su, Comparative analysis of architecturally tuned nanostructured MXENE/PVDF composites for electromagnetic shielding, *ACS Appl. Nano Mater.*, 2023, **6**, 23292–23302.

4 S. Habibpour, K. Zarshenas, M. Zhang, M. Hamidinejad, L. Ma, C. B. Park and A. Yu, Greatly enhanced electromagnetic interference shielding effectiveness and mechanical properties of Polyaniline-Grafted TI3C2TX MXENE–PVDF composites, *ACS Appl. Mater. Interfaces*, 2022, **14**, 21521–21534.

5 V. B and U. R. M, A free-standing CaO infused PVdF-HFP/PMMA polymer-nanocomposite as solid-state electrolytes for energy storage applications, *Ionics*, 2024, **30**, 6061–6071.

6 S. Jia, Z. Yan, Y. Zhu, Q. Zhang, X. Zhang, P. Coates, W. Liu and Z. Zhao, Distinct strategy for the improvement of conductivity and electromagnetic shielding properties of MWCNTs/PLA/PBS composites: Synergistic effects of double percolation structure and UV aging, *Polym. Compos.*, 2023, **44**, 2816–2835.

7 J. Song, K. Xu, J. He, H. Ye and L. Xu, Three-dimensional graphene/carbon nanotube electromagnetic shielding composite material based on melamine resin foam template, *Polym. Compos.*, 2023, **44**, 2836–2845.

8 S. Lee, M. Kim, V. A. Cao, J. Park, I.-J. Yoon, P. Park and J. Nah, High performance flexible electromagnetic interference shielding material realized using ZnO nanorod decorated polyvinylidene fluoride (PVDF)-MXene composite nanofibers, *J. Mater. Chem. C*, 2023, **11**, 1522–1529.

9 M. Naguib, M. Kurtoglu, V. Presser, J. Lu, J. Niu, M. Heon, L. Hultman, Y. Gogotsi and M. W. Barsoum, Two-Dimensional nanocrystals produced by exfoliation of TI3ALC2, *Adv. Mater.*, 2011, **23**, 4248–4253.

10 L. Liu, R. Guo, J. Gao, Q. Ding, Y. Fan and J. Yu, Mechanically and environmentally robust composite nanofibers with embedded MXene for wearable shielding of electromagnetic wave, *Compos. Commun.*, 2022, **30**, 101094.

11 J. Ahmad, A. Maryam, H. S. Manzoor, N. Nasir, Y. Nawab and H. S. Ahmad, Enhancement of EMI shielding effectiveness in carbon fiber-reinforced composite structures impregnated with MWCNT and Fe2O3 nanofillers through optimized laminating sequences, *Mater. Sci. Eng., B*, 2025, **313**, 117980.

12 Z. Han, Y. Niu, X. Shi, D. Pan, H. Liu, H. Qiu, W. Chen, B. B. Xu, Z. M. El-Bahy, H. Hou, E. R. Elsharkawy, M. A. Amin, C. Liu and Z. Guo, MXENE@C-MWCNT adhesive silica nanofiber membranes enhancing electromagnetic interference shielding and thermal insulation performance in extreme environments, *Nano-Micro Lett.*, 2024, **16**(1), 195.

13 S. Kumar, S. M. Z. Mehdi, M. Taunk, S. Kumar, A. Aherwar, S. Singh and T. Singh, Synergistic impacts on properties, stability, and applications of MXEnes *via* polymer integration, *J. Mater. Chem. A*, 2025, **13**(16), 11050–11113.

14 S. Araby, N. Saber, X. Ma, N. Kawashima, H. Kang, H. Shen, L. Zhang, J. Xu, P. Majewski and J. Ma, Implication of multi-

walled carbon nanotubes on polymer/graphene composites, *Mater. Des.*, 2014, **65**, 690–699, DOI: 10.1016/j.matdes.2014.09.069.

15 R. Verma, P. Thakur, A. Chauhan, R. Jasrotia and A. Thakur, A review on MXene and its' composites for electromagnetic interference (EMI) shielding applications, *Carbon*, 2023, **208**, 170–190.

16 Z. Yan, Y. Ding, M. Huang, J. Li, Q. Han, M. Yang and W. Li, MXENE/CNTs/Aramid aerogels for electromagnetic interference shielding and joule heating, *ACS Appl. Nano Mater.*, 2023, **6**, 6141–6150.

17 K. Rajavel, S. Luo, Y. Wan, X. Yu, Y. Hu, P. Zhu, R. Sun and C. Wong, 2D Ti3C2Tx MXene/polyvinylidene fluoride (PVDF) nanocomposites for attenuation of electromagnetic radiation with excellent heat dissipation, *Composites, Part A*, 2019, **129**, 105693.

18 H. Wang, K. Zheng, X. Zhang, T. Du, C. Xiao, X. Ding, C. Bao, L. Chen and X. Tian, Segregated poly(vinylidene fluoride)/MWCNTs composites for high-performance electromagnetic interference shielding, *Composites, Part A*, 2016, **90**, 606–613.

19 C. Sun, W. Peng, M. Huang, K. Zhao and M. Wang, Constructing high-efficiency microwave shielding networks in multi-walled carbon nanotube/poly(ε-caprolactone) composites by adding carbon black and graphene nanoplates, *Polym. Int.*, 2023, **72**, 619–628.

20 G. Weng, J. Li, M. Alhabeb, C. Karpovich, H. Wang, J. Lipton, K. Maleski, J. Kong, E. Shaulsky, M. Elimelech, Y. Gogotsi and A. D. Taylor, Layer-by-Layer assembly of Cross-Functional semi-transparent MXENE-Carbon nanotubes composite films for Next-Generation electromagnetic Interference shielding, *Adv. Funct. Mater.*, 2018, **28**(44), 1803360.

21 B. Zhao, C. Zhao, M. Hamidinejad, C. Wang, R. Li, S. Wang, K. Yasamin and C. B. Park, Incorporating a microcellular structure into PVDF/graphene–nanoplatelet composites to tune their electrical conductivity and electromagnetic interference shielding properties, *J. Mater. Chem. C*, 2018, **6**, 10292–10300.

22 H. Zhang, G. Zhang, J. Li, X. Fan, Z. Jing, J. Li and X. Shi, Lightweight, multifunctional microcellular PMMA/Fe 3 O 4 @MWCNTs nanocomposite foams with efficient electromagnetic interference shielding, *Composites, Part A*, 2017, **100**, 128–138.

23 L. Liang, P. Xu, Y. Wang, Y. Shang, J. Ma, F. Su, Y. Feng, C. He, Y. Wang and C. Liu, Flexible polyvinylidene fluoride film with alternating oriented graphene/Ni nanochains for electromagnetic interference shielding and thermal management, *Chem. Eng. J.*, 2020, **395**, 125209.

24 A. A. Al-Ghamdi, F. El-Tantawy, N. A. Aal, E. H. El-Mossalamy and W. E. Mahmoud, Stability of new electrostatic discharge protection and electromagnetic wave shielding effectiveness from poly (vinyl chloride)/graphite/nickel Nano conducting composites, *Polym. Degrad. Stab.*, 2009, **94**(6), 980–986, DOI: 10.1016/j.polymdegradstab.2009.02.012.

25 P. Rani, B. Ahamed and K. Deshmukh, Dielectric and electromagnetic interference shielding properties of zeolite13Xand carbon black nanoparticles based PVDF nanocomposites, *J. Appl. Polym. Sci.*, 2021, **138**(13), DOI: 10.1002/app.50107.

26 J. Cheng, C. Li, Y. Xiong, H. Zhang, H. Raza, S. Ullah, J. Wu, G. Zheng, Q. Cao, D. Zhang, Q. Zheng and R. Che, Recent advances in design strategies and multifunctionality of flexible electromagnetic interference shielding materials, *Nano-Micro Lett.*, 2022, **14**, 80.

27 G. Weng, J. Li, M. Alhabeb, C. Karpovich, H. Wang, J. Lipton, K. Maleski, J. Kong, E. Shaulsky, M. Elimelech, Y. Gogotsi and A. D. Taylor, Layer-by-Layer assembly of Cross-Functional semi-transparent MXENE-Carbon nanotubes composite films for Next-Generation electromagnetic Interference shielding, *Adv. Funct. Mater.*, 2018, **28**(44), 1803360.

28 B. Luo, X. Wang, H. Wang, Z. Cai and L. P. Li, VDF-HFP)/PMMA flexible composite films with enhanced energy storage density and efficiency, *Compos. Sci. Technol.*, 2017, **151**, 94–103, DOI: 10.1016/j.compscitech.2017.08.013.

29 A. Ryu, H. Yim, S. Yoo, J. Park, D. Lee, J. Y. Lee, H. Song, S. H. Baek, S. Nahm and J. Choi, Layer-Controlled Perovskite 2D Nanosheet interlayer for the energy storage performance of nanocomposites, *Small*, 2023, **19**(28), 2300526.

30 J.-W. Zha, M.-S. Zheng, B.-H. Fan and Z.-M. Dang, Polymer-based dielectrics with high permittivity for electric energy storage: A review, *Nano Energy*, 2021, **89**, 106438, DOI: 10.1016/j.nanoen.2021.106438.

31 X. Li, Y. Wang, Y. Rao, X. Ma, Y. Yang and J. Zhang, Enhanced Energy Storage in PVDF-Based Nanocomposite Capacitors through (00l)-Oriented BaTiO3 Single-Crystal Platelets, *ACS Appl. Mater. Interfaces*, 2024, **16**(21), 27785–27793, DOI: 10.1021/acsami.4c04340.

32 Y. Wang, P. He and F. Li, Preparation and dielectric property of MWCNT/CCTO/PVDF composite film, *Mater. Res. Express*, 2018, **5**(6), 066304, DOI: 10.1088/2053-1591/aaca1a.

33 Y. Yang, C.-L. Luo, X.-D. Chen and M. Wang, Sustainable electromagnetic shielding graphene/nanocellulose thin films with excellent joule heating and mechanical properties *via in situ* mechanical exfoliation and crosslinking with cations, *Compos. Sci. Technol.*, 2023, **233**, 109913.

34 M. Tiwari, R. Joshi and I. Lahiri in *Polymer Nanocomposites for EMI Shielding Applications*, pp. 105–151, 2024, DOI: 10.1007/978-981-97-2104-7_5.

35 K. Rajavel, S. Luo, Y. Wan, X. Yu, Y. Hu, P. Zhu, R. Sun and C. Wong, 2D Ti3C2Tx MXene/polyvinylidene fluoride (PVDF) nanocomposites for attenuation of electromagnetic radiation with excellent heat dissipation, *Composites, Part A*, 2019, **129**, 105693.

36 L. P. Yu, X. H. Zhou, L. Lu, L. Xu and F. J. Wang, MXENE/Carbon Nanotube Hybrids: Synthesis, structures, properties, and applications, *ChemSusChem*, 2021, **14**, 5079–5111, DOI: 10.1002/cssc.202101614.

37 J. FitzPatrick, S. Bera, A. Inman, A. Cabrera, T. Zhang, T. Parker, B. S. Mohammadlou, I. Roslyk, S. Ippolito, K. Shevchuk, S. A. Kadam, N. R. Pradhan and Y. Gogotsi, Record efficiency of Β-Phase PVDF-MXENE composites in

Thin-Film dielectric capacitors, *Adv. Mater.*, 2025, **37**(12), 2419088.

38 R. Gregorio Jr and M. Cestari, Effect of crystallization temperature on the crystalline phase content and morphology of poly (vinylidene fluoride), *J. Polym. Sci., Part B:Polym. Phys.*, 1994, **32**, 859–870.

39 C. Likitaporn, M. Okhawilai, P. Kasemsiri, J. Qin, P. Potiyaraj and H. Uyama, High electrolyte uptake of MXene integrated membrane separators for Zn-ion batteries, *Sci. Rep.*, 2022, **12**(1), 19915.

40 J.-K. Yuan, W.-L. Li, S.-H. Yao, Y.-Q. Lin, A. Sylvestre and J. Bai, High dielectric permittivity and low percolation threshold in polymer composites based on SiC-carbon nanotubes micro/nano hybrid, *Appl. Phys. Lett.*, 2011, **98**, 032901.

41 B. A. Alshammari, F. S. Al-Mubaddel, M. R. Karim, M. Hossain, A. S. Al-Mutairi and A. N. Wilkinson, Addition of graphite filler to enhance electrical, morphological, thermal, and mechanical properties in poly (Ethylene terephthalate): experimental characterization and material modeling, *Polymers*, 2019, **11**, 1411.

42 R. Ram, V. Soni and D. Khastgir, Electrical and thermal conductivity of polyvinylidene fluoride (PVDF) – Conducting Carbon Black (CCB) composites: Validation of various theoretical models, *Composites, Part B*, 2020, **185**, 107748.

43 N. K. Nath, R. R. Mohanta, R. K. Parida, B. N. Parida and N. C. Nayak, Improving the energy storage efficiency and power density of polymer blend in combination with Ti3C2Tx for energy storage devices, *Mater. Today Chem.*, 2024, **41**, 102338.

44 P. Sivaraj, K. P. Abhilash, B. Nalini, P. Perumal and P. C. Selvin, Free-standing, high Li-ion conducting hybrid PAN/PVdF/LiClO4/Li0.5La0.5TiO3 nanocomposite solid polymer electrolytes for all-solid-state batteries, *J. Solid State Electrochem.*, 2020, **25**, 905–917.

45 Q. Zhang, J. Cui, S. Zhao, G. Zhang, A. Gao and Y. Yan, Development of Electromagnetic-Wave-Shielding Polyvinylidene Fluoride–TI3C2TX MXENE–Carbon nanotube composites by improving impedance matching and conductivity, *Nanomaterials*, 2023, **13**, 417.

46 J. FitzPatrick, S. Bera, A. Inman, A. Cabrera, T. Zhang, T. Parker, B. S. Mohammadlou, I. Roslyk, S. Ippolito, K. Shevchuk, S. A. Kadam, N. R. Pradhan and Y. Gogotsi, Record efficiency of B-Phase PVDF-MXENE composites in Thin-Film dielectric capacitors, *Adv. Mater.*, 2025, **37**(12), 2419088.

47 Y. Hu, D. Li, L. Wu, J. Yang, X. Jian and Y. Bin, Carbon nanotube buckypaper and buckypaper/polypropylene composites for high shielding effectiveness and absorption-dominated shielding material, *Compos. Sci. Technol.*, 2019, **181**, 107699.

48 J. Song, K. Xu, J. He, H. Ye and L. Xu, Three-dimensional graphene/carbon nanotube electromagnetic shielding composite material based on melamine resin foam template, *Polym. Compos.*, 2023, **44**, 2836–2845.

49 H. J. Sim, D. W. Lee, H. Kim, Y. Jang, G. M. Spinks, S. Gambhir, D. L. Officer, G. G. Wallace and S. J. Kim, Self-healing graphene oxide-based composite for electromagnetic interference shielding, *Carbon*, 2019, **155**, 499–505.

50 J.-R. Tao, C.-L. Luo, M.-L. Huang, Y.-X. Weng and M. Wang, Construction of unique conductive networks in carbon nanotubes/polymer composites *via* poly(ε-caprolactone) inducing partial aggregation of carbon nanotubes for microwave shielding enhancement, *Composites, Part A*, 2022, **164**, 107304.

51 B. Zhao, Y. Du, Z. Yan, L. Rao, G. Chen, M. Yuan, L. Yang, J. Zhang and R. Che, Structural Defects in Phase-Regulated High-Entropy Oxides toward Superior Microwave Absorption Properties, *Adv. Funct. Mater.*, 2022, **33**(1), 2209924.

52 B. Zhao, Z. Yan, Y. Du, L. Rao, G. Chen, Y. Wu, L. Yang, J. Zhang, L. Wu, D. W. Zhang and R. Che, High-Entropy enhanced microwave attenuation in titanate perovskites, *Adv. Mater.*, 2023, **35**(11), 2210243.

53 S. Chauhan, P. N. Mohan, K. C. J. Raju, S. Ghotia, N. Dwivedi, C. Dhand, S. Singh and P. Kumar, Free-standing polymer/multiwalled carbon nanotubes composite thin films for high thermal conductivity and prominent EMI shielding, *Colloids Surf., A*, 2023, **673**, 131811.

54 J. B. Anooja, K. S. Dijith, K. P. Surendran and G. Subodh, A simple strategy for flexible electromagnetic interference shielding: Hybrid rGO@CB-Reinforced polydimethylsiloxane, *J. Alloys Compd.*, 2019, **807**, 151678.

55 S. S. Hota, D. Panda, S. B. Bhoobash, S. Mishra, L. Biswal, S. Joshi, A. Shukla, D. Das, R. N. P. Choudhary and S. K. S. Parashar, Absorption-Dominant electromagnetic Interference shielding of polymer nanocomposite PVDF/LINBO3 for High-Frequency microwave application, *ACS Appl. Electron. Mater.*, 2025, **7**(10), 4481–4492.

56 H. Ye, C. Xu, N. Meng, Z. Meng and L. Xu, High energy density and charge–discharge efficiency of uniaxial stretched poly (vinylidene fluoride-hexafluoropropylene) film with electroactive phase conversion, *J. Mater. Sci.:Mater. Electron.*, 2018, **29**, 6619–6631.

57 N. K. Nath, R. Parida, B. N. Parida and N. C. Nayak, Synergistic effects of MWCNT–MXENE nanohybrids on dielectric and ferroelectric properties of PVDF/PMMA blend composites, *ACS Appl. Electron. Mater.*, 2025, **7**(3), 1252–1266.

58 H. Luo, X. Zhou, C. Ellingford, Y. Zhang, S. Chen, K. Zhou, D. Zhang, C. R. Bowen and C. Wan, Interface design for high energy density polymer nanocomposites, *Chem. Soc. Rev.*, 2019, **48**, 4424–4465.